that these conducting edges are indeed the helical modes expected at the boundary of a 2D topological insulator. Helical edges should have a length-independent quantized resistance for sample lengths shorter than a characteristic spin scattering length, and indeed edge resistances close to the expected values were reported by several groups[6,8,13]. However, the crossover from a length dependent resistance for long samples to resistance quantization for small samples offers a simple experimental check for helical character that has yet to be mapped out. The lack of a consistent map between the trivial/inverted transition and the appearance of edge transport means that reports to date must be taken as circumstantial but not direct evidence for helical edge states.

Here we report measurements of edge channels conduction in InAs/GaSb samples that can be tuned *in situ* between trivial and inverted regimes, combining transport methods with scanned spatial characterization using a superconducting quantum interference device (SQUID). The primary result of this experiment is that when the sample is tuned via top and back gates into the trivial insulating regime, conductance is totally suppressed through the bulk, but transport remains along the sample edges. Despite the fact that these edges are observed in a regime where no helical states are expected, at a superficial level their conductance characteristics are similar to those previously reported as evidence for the QSH state in InAs/GaSb. Resistance plateaus at apparently-quantized values [Sec. IV B] are observed in an H bar geometry that was designed to resemble devices described in existing literature[8,11]. Looking more carefully, however, the edge resistance scales linearly with edge length even in the limit of very short edges, in contradiction to the single-channel conductance of a helical edge. Furthermore, the edge channel resistance per unit length is very close to earlier reports of helical edge channels[8,11]. These observations imply a burden on future QSH experiments in InAs/GaSb to confirm not only the helical character of edges in the inverted regime, but also the absence of conducting edges in the trivial regime that might otherwise conduct in parallel with helical modes.

The paper is organized as follows: First, experimental and fabrication details of the measurements are provided. Macroscopic transport measurements in Hall bar and Corbino geometries map out trivial and inverted regimes of gate voltage. Taken together, these measurements show that conduction in the trivial regime is entirely along the sample edges, with an immeasurably small contribution from the bulk.

The length dependence of the edge resistance is measured using mesoscopic two-terminal devices. The resistance falls well below the expected $h/2e^2$ for edge segments shorter than one micron. We proceed with an investigation of H bars and microscopic (μ) Hall bars with dimensions very similar to those reported in earlier work[8,11]. Here we note the remarkable coincidence that typical edge resistance per unit length in these samples gives resistances near those expected from quantization for the same sample geometries reported in the literature, despite the fact that our measurements are manifestly performed in the trivial regime. The paper concludes with a scanning probe demonstration of edge conduction in the trivial regime. Edge conduction is enhanced also in the inverted regime, but there it is masked by a bulk contribution.

II. EXPERIMENTAL DETAILS

Experiments were performed on three different wafers, labeled A, B and C. The structures were grown by molecular beam epitaxy on a conductive GaSb substrate, which served as a global back gate[14]. From the substrate to the surface, all three structures consisted of a GaSb/AlSb insulating buffer, a 5 nm GaSb QW, an InAs QW (10.5 nm for wafer A and B, 12.5 nm for wafer C), a 50 nm AlSb insulating barrier and a 3 nm GaSb capping layer. Transport experiments were performed on wafers A and B, although measurements reported here (Figs 1-7) are from wafer A only. Analogous measurements on wafer B gave consistent results. Scanning SQUID measurements (Figs. 8 and 9) were performed on Wafer C, previously characterized by transport measurements in Ref. 9. Magnetotransport measurements reported here and elsewhere[9] confirm that the bandstructures of wafers A, B, and C are trivial at $V_{\rm BG} = 0$.

The quality of the material studied here is attested to by the high electron mobility compared to samples in previous reports[3–8]. The mobility versus density characteristic of wafer C was measured in Refs. 9 and 14, yielding mobility values in excess of 50 $\mathrm{m^2V^{-1}s^{-1}}$ for an electron density of 10^{16} $\mathrm{m^{-2}}$. The mobility in wafer A and B follows a similar dependence on density as wafer C, with an overall decrease by about a factor of two.

Devices were patterned by conventional optical and electron beam lithography techniques and wet etching. Devices shown in Figs. 1 and 3 were etched using a sequence of selective etchants[15], the other devices with a conventional III-V semiconductor etchant[14]. The two recipes gave consistent results. Ohmic contacts were obtained by etching the samples down to the InAs QW and depositing Ti/Au electrodes. Top gates were defined by covering the samples with a thin ($\leq$ 80 nm) Al_2O_3 or HfO_2 insulating layer grown by atomic layer deposition and a patterned Ti/Au electrode. The one exception to this was the Corbino disk presented in Fig. 3, for which the insulator consisted of a 90 nm sputtered layer of Si_3N_4. In many devices the back gates leaked when more than $\pm$100mV was applied, presumably due to damage during processing. These leaky devices were only operated at zero backgate voltage, where the resistance to the backgate was at least 10 GΩ. Except where specified, transport experiments were performed in dilution refrigerators at a temperature of less than 50 mK with standard low frequency lock-in techniques. Additional details regarding the wafer growth, sample fabri-

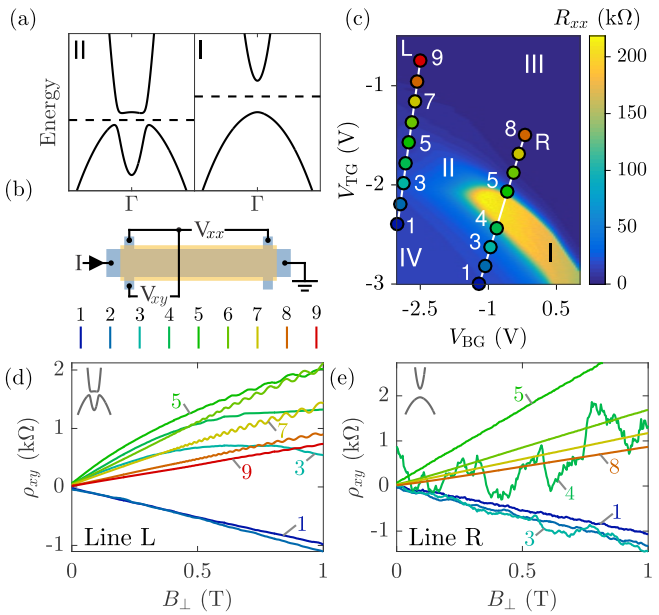

FIG. 1. (a) Schematic representation of the InAs/GaSb band structure for inverted (left) and trivial (right) regime. We interpret region II and region I in (c) as the situation when the Fermi energy (dashed line) lies in the gap in the inverted and trivial case, respectively. Through the rest of the paper we will use these schematic bandstructure representations to indicate weather a measurement is performed in the regime of region II or I [for example in (d) and (e) respectively]. (b) Schematic representation of the macroscopic Hall bar and the electrical setup used to measure the longitudinal resistance R_{xx} in (c) and the transverse resistivity ρ_{xy} (d,e). (c) Top and backgate voltage dependence of R_{xx} (bias current $I = 5$ nA). $\rho_{xy}(B_\perp)$ is measured at each of the locations marked by circles along the lines L and R, shown in (d) and (e) respectively (bias current $I = 10$ nA).

cation and basic electrical characterization are provided in Refs. 9 and 14.

III. TRANSPORT IN MACROSCOPIC SAMPLES

A. Magnetotransport Data

The gate-voltage induced crossover between trivial and topological regimes is clearly seen in magnetoresistance measurements performed on a large Hall bar made from wafer A [Fig. 1(b)]. The Hall bar width (20 μm) was large enough so that adjacent mesa edges were presumably separated by a pristine bulk unperturbed by possible band bending or electrostatic effects near an etched edge. The separation of lateral contacts (100 μm) was much longer than any edge scattering lengths reported in the literature. Positive backgate voltages, $V_{\rm BG}$, together with negative topgate voltages, $V_{\rm TG}$, raise the electron (conduction) band while lowering the hole (valence) band, creating the band structure of a trivial insulator. When the Fermi energy is tuned into the resulting energy gap, the longitudinal resistance rises to hundreds of kΩ or larger [region I in Fig. 1(c)]. The inverted regime emerges for negative $V_{\rm BG}$ simultaneous with more positive $V_{\rm TG}$, that is, when the valence band maximum is driven above the conduction band minimum. When the Fermi energy is tuned into the hybridization gap, [region II in Fig. 1(c)], the resistance is much smaller compared to region I, consistent with previous measurements[9]. Driving the Fermi energy out of the gap, into the conduction (valence) band, yields electron (hole) dominated region transport corresponding to regions III (IV).

Monitoring the magnetic field dependence of the transverse resistivity, $\rho_{xy}(B_\perp)$, offers a signature of the gate induced transition from trivial to inverted band structure[9]. In the trivial regime, carriers on either side of the charge neutrality point are either electron-like or hole-like, giving rise to ρ_{xy} that is linear in $B_\perp$[16]. The inverted regime, on the other hand, involves an overlap of electron-like and hole-like carriers near the charge neutrality point, giving rise to ρ_{xy} that is non-monotonic in $B_\perp$. Moving the Fermi energy across the gap in the trivial regime [line R in Fig. 1(c)] indeed yields $\rho_{xy}(B_\perp)$ traces that are linear, with the slope passing from negative in the pure hole regime (point 1) to positive in the pure electron regime (point 8) [Fig. 1(e)]. The charge neutrality point along line R (point 4) gives $\rho_{xy}(B_\perp)$ with large fluctuations and no net slope [Fig. 1(e)]. A similar set of traces along line L [Fig. 1(c)], which crosses the inverted band gap, displays the non-monotonic behavior near the charge neutrality point indicative of simultaneous transport of electron- and hole-like carriers [Fig. 1(d)]. Based on this interpretation, representations of the bandstructure are shown as figure insets throughout this paper in order to clarify which measurements are performed in topological versus trivial regimes [e.g. Fig. 1(d,e)].

Previous measurements[9] mapped out the front and back gate dependence of resistivity in the higher-mobility sample C, and correlated features in the zero field resistivity with band structure alignments determined by magnetoresistance. Consistent with the analysis in Ref. 9, the resistivity peak at $V_{\rm TG} \sim -2.1$ V in Fig. 1(c) marks the crossover from exclusively hole-like transport ($V_{\rm TG} \lesssim -2.1$ V) to the overlap region including both conduction and valence bands ($V_{\rm TG} \gtrsim -2.1$ V). The lower mobility of sample A, compared to sample C, precludes the observation in Fig. 1(c) of an additional resistance peak at the charge neutrality point in the inverted regime. Such a feature might appear driving the sample deeper in the hybridization regime.

In the hybridization gap of the inverted regime (region II) transport is expected to occur along helical edge channels, ballistic over short distances. The edge channels scattering length has been quantified in previous work as several microns[6,8]. Along a 100 μm segment of Hall bar, an edge channel resistance exceeding h/e^2 by at least one order of magnitude is therefore expected, whereas the

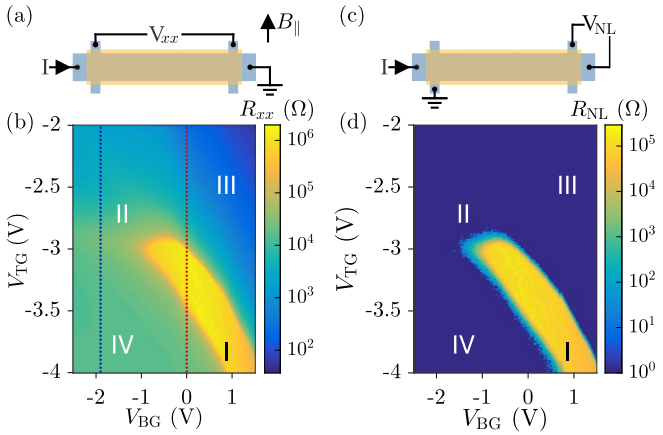

FIG. 2. (a,c) Schematic representation of the Hall bar geometry and electrical configuration for measuring local longitudinal resistance R_{xx} (b) and non-local resistance R_{NL} (d). The direction of the in-plane magnetic field used in Fig. 5 is indicated. (b) Longitudinal resistance R_{xx} as a function of back gate and top gate voltages. Dashed lines indicate the back gate voltages where temperature [Fig. 4(d)] and in-plane magnetic field (Fig. 5) measurements were performed. (d) Non-local resistance R_{NL} as a function of back gate and top gate voltages. Note: the color scale in (d) is limited to a minimum of 1 Ω.

observed resistance peak in region II is around 40 kΩ. This inconsistency may be resolved by including a residual bulk conduction that adds in parallel with the edge channels. One may ask whether a similar explanation is responsible for the residual conductivity in the trivial insulating regime. As we will show in the following, the finite resistance observed in Region I is instead due to conductive edge channels propagating over the sample perimeter.

B. Non-Local Measurements

The device geometry described in Fig. 1(b) measures transport through the bulk in parallel with the edges that connect voltage probes. In order to separate bulk and edge contributions, we consider two different measurement geometries, both implemented in macroscopic samples. First, we probe edge conduction by measuring a Hall bar, nominally identical to that of Fig. 1, in a non-local geometry; second, we isolate bulk conduction by measuring Corbino disks made from the same wafer.

When current and voltage probes for the Hall bar device geometry from Fig. 1(b) are rearranged to a non-local configuration, in which the voltage measurement is performed far from the expected (bulk) current path, the contribution of bulk conduction to the voltage signal is vanishingly small. Quantitatively, the non-local resistance $R_{NL} \equiv dV_{nl}/dI$ due only to diffusive current spreading through the bulk is expected theoretically[17] to be suppressed by a factor of $e^{-\pi S} \sim 10^{-7}$ compared to R_{xx}, where $S = 5$ is the number of squares between current path and non-local voltage probes. On the other hand, edge currents propagating around the sample perimeter would pass the voltage contacts directly and give a sizeable signal.

A comparison of local [Fig. 2(a,b)] and non-local [Fig. 2(c,d)] measurements can therefore distinguish bulk-dominated and edge-dominated transport. In particular, the non-local resistance R_{NL} in region I is within an order of magnitude of R_{xx}, whereas in regions II, III, IV R_{NL} is at least four orders of magnitude smaller. Similar measurements for different contact configurations, all around the perimeter of the Hall bar, gave consistent non-local responses. This demonstrates that region I is dominated by edge transport, whereas II, III, IV are dominated by bulk conduction. Note that the Hall bars in Figs. 1 and 2 are made from the same wafer, and have the same geometry, but R_{xx} in region I is nearly an order of magnitude larger in Fig. 2(b) compared to Fig. 1(c). In addition to sample-to-sample variability, this difference may be due to much lower bias currents applied in the insulating region for Fig. 2(c) measurements (10 pA) compared to 5 nA in Fig. 1(c)[18].

C. Corbino Disks

The non-local measurements presented above demonstrate that transport in region I is dominated by edge conduction, but do not directly quantify the degree to which bulk conduction is suppressed ($\sigma_{xx} \to 0$). In order to do that, we turn to measurements performed in a Corbino geometry [Fig. 3(b) inset], in which the current flows exclusively through a ring-shaped bulk between concentric contacts and no sample edge connects source and drain. A global top gate overlapping the metallic contacts (but separated by dielectric) tunes the bulk conductance homogeneously. Measurements in Figs. 3 and 4 were performed on two different Corbino disks in a two-probe configuration. The known series resistance in the cryostat was subtracted from the data.

The first Corbino ring (Fig. 3), has internal and external radii of 100 μm and 160 μm respectively. In this sample, confirmation of the trivial-to-inverted transition is seen in the data of Fig. 3(a), showing the inverse of the Corbino conductivity $1/\sigma_{xx}$ at a fixed out-of-plane field of 1.5 T. In the electron regime, clear Shubnikov-de Haas (SdH) oscillations map out contours of constant electron density. Because of the lower mobility and higher effective mass, the SdH oscillations are not visible in the hole regime at the same magnetic field. The slope change of the SdH oscillations, marked in Fig. 3(c) with a black line, is interpreted as the transition from the trivial to the inverted regime. Following the arguments of Ref. 9, the coexistence of electrons and holes to the left of the black line results in a decreased back gate capacitance to the electron gas with respect to the right side of the line, where only electrons are present. Similarly, the reduction

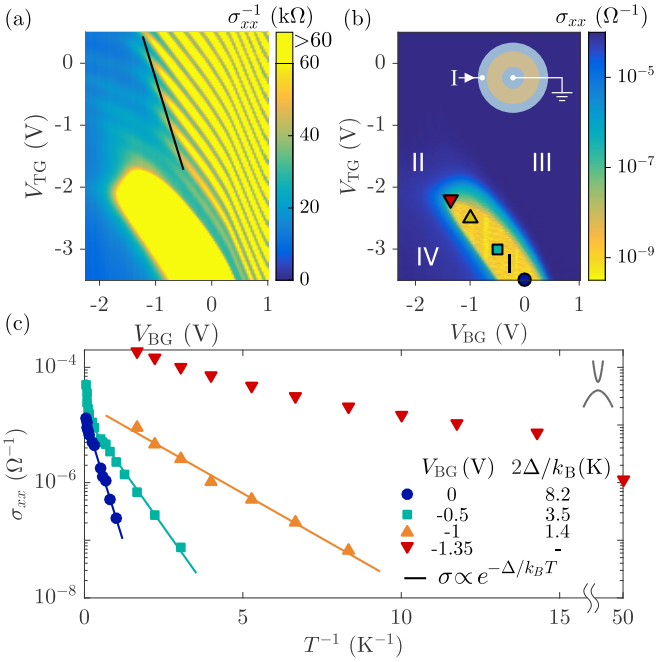

FIG. 3. (a) Inverse of the longitudinal conductivity, σ_{xx}^{-1}, of the Corbino disk in an out-of-plane field $B_\perp = 1.5$ T. The black line marks the slope change in the SdH oscillations, associated to the onset of hole conduction. (b) Longitudinal conductivity σ_{xx} measured in a Corbino disk as a function of top gate and back gate voltage. Markers indicate the regimes where the temperature dependence of (c) was taken. Inset: schematic representation of the Corbino geometry. (c) Temperature dependence of the bulk conductivity (markers) together with fits to the Arrhenius law (solid line) at each back gate voltages.

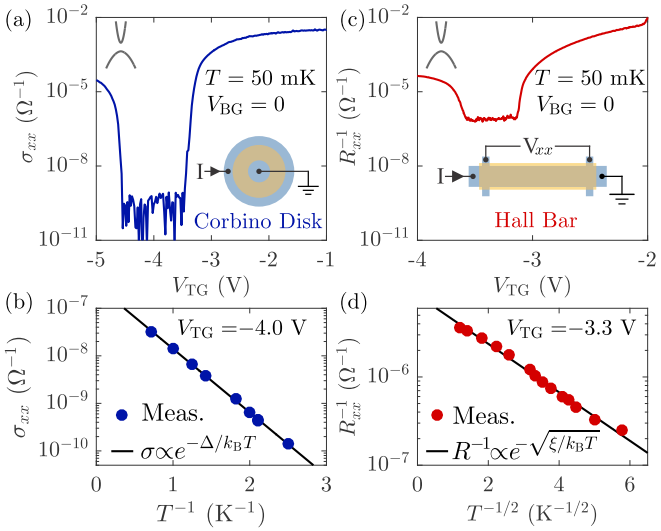

FIG. 4. (a) Conductivity in the Corbino disk at $V_{BG} = 0$ as a function of V_{TG}. Inset: schematic representation of the Corbino disk. (b) Temperature dependence of the conductivity in the Corbino disk (dots) as a function of T^{-1} and a fit to the Arrhenius equation (solid line). (c) Inverse of the longitudinal resistance R_{xx} measured in the Hall bar at $V_{BG} = 0$ as a function of V_{TG}. Inset: schematic representation of the measurement setup. (d) Temperature dependence of the Hall bar inverse resistance (dots) together with a fit to the variable range hopping equation (solid line). The horizontal axis is plotted as $T^{-1/2}$ to highlight the consistency with the extracted fit parameter $\alpha = 2$.

in the visibility of the oscillations can be attributed to the onset of hole conduction in parallel to electron system.

When the out-of-plane magnetic field is reduced to zero, the gate voltage map of the conductivity σ_{xx} of the Corbino sample [Fig. 3(b)] looks qualitatively similar to the resistance of the Hall bar [Fig. 1(c)]. At a quantitative level, however, the resistance of region I in the Hall bar is four orders of magnitude lower than the inverse conductivity of the Corbino sample. This can be understood from the fact that the Hall bar geometry in Fig. 1(b) measures transport via the bulk in parallel with edges that connect V_{xx} voltage probes, whereas the source and drain for the Corbino disk are coupled only via bulk, with no edges. The substantially larger resistance of the Corbino sample therefore indicates that transport in the Hall bar is dominated by conducting edge channels, while the bulk is strongly insulating (GΩ or higher at low temperature).

D. Temperature Dependence

Bulk conductivity in the trivial state is strongly temperature dependent. The evolution of the Corbino conductivity, as a function of temperature, extracted for different top gate and back gate voltages from Fig. 3(b) is shown in Fig. 3(c). Good agreement with Arrhenius law $\sigma_{xx} \propto \exp(-\Delta/k_BT)$, with 2Δ the energy gap, over more than two orders of magnitude in resistance [Fig. 3(c)] indicates activated transport with $2\Delta/k_B$ ranging from 1.4 K to 8 K. The energy gap increases for more positive back gate voltages, $V_{BG} \geq -1$ V [Fig. 3(c)]. This behavior is qualitatively, but not quantitatively, consistent with a parallel plate capacitor model[9], as discussed in Sec. VI. The temperature dependence for $V_{BG} = -1.35$ V is not well fit by an Arrhenius law or a model describing variable range hopping. This is presumably due to the onset of bulk conduction close to the band crossing point.

Similar results were obtained in the second Corbino ring, with internal and external radii of 50 μm and 120 μm respectively. The gate voltage dependence of this device was limited to $V_{BG} = 0$ due to backgate leakage. Compatibly with the measurement in Fig. 3(b), the insulating region was characterized by a very low minimum conductivity (experimental noise limited), indicating a strongly insulating bulk [Figs. 4(a)]. A fit to an Arrhenius law [Figs. 4(b)] gives a $V_{BG} = 0$ energy gap of $2\Delta/k_B = 6.2$ K, consistent with the previous sample.

Compared to Corbino measurements, the temperature dependence of the conductivity in the Hall bar geometry was much weaker, and inconsistent with the Arrhenius

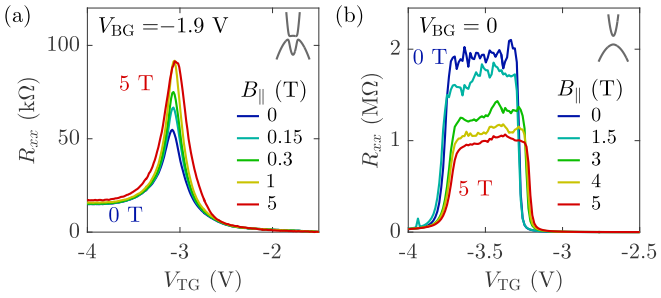

FIG. 5. (a) Hall bar resistance from Fig. 2(c) at $V_{BG} = -1.9$ V for different values of in-plane magnetic field. The resistance peak is associated to the onset of the conduction band in the hole regime. (b) As in (a), for $V_{BG} = 0$. The resistance peak marks the trivial gap with edge channel conduction. The field direction in (a) and (b) is indicated in Fig. 2(a).

law observed in the bulk [Fig. 4(b)]. Figure 4(d) shows the inverse longitudinal resistance R_{xx}^{-1} measured in the Hall bar of Fig. 2 for $V_{BG} = 0$ and $T = 50$ mK. As already noted, the minimum conductance in the Hall bar is four orders of magnitude higher than in the Corbino. Fitting the Hall bar temperature dependence to a more general equation, $R_{xx} \propto \exp(\xi/k_B T)^{1/\alpha}$, with ϵ and α as fit parameters, yielded $\alpha = 2.0 \pm 0.5$ compared with $\alpha = 1$ for simple activated behavior. The value $\alpha = 2$ is consistent with variable range hopping in one dimension or Coulomb dominated hopping in one or two dimensions[19]. Fixing $\alpha = 2$, we obtain $\xi/k_B = (0.4 \pm 0.04)$ K. The insulating temperature dependence of edge resistance observed in these measurements, as well as the strong dependence on bias current or voltage observed at very low temperatures, are qualitatively consistent with recent reports of Luttinger liquid behavior in InAs/GaSb edge modes[18]. However, the precise functional forms used in Ref. 18 were found not to fit our data.

E. In-Plane Magnetic Field Dependence

The effect of an in-plane field, $B_\parallel$, can be particularly revealing in the case of InAs/GaSb, as it allows one to distinguish between trivial and inverted phases. The in-plane magnetic field shifts the electron and hole band relative to each other in momentum, quenching the hybridization gap in the inverted regime but leaving the trivial gap largely unaltered[9,20]. In the present experiment, however, the quenching of the hybridization gap in the inverted regime cannot be clearly seen due to the large residual bulk conduction that mask the charge neutrality point. Figure 5(a) shows the in-plane magnetoresistance for gate voltage settings ($V_{BG} = -1.9$ V) that give rise to a inverted band alignment. As already noted in Sec. III A, the resistance peak in Fig. 5(a) is associated with the onset of the conduction band in the hole regime, not with the charge neutrality point. The large positive magnetoresistance at low field ($B_\parallel < 1$ T) cannot be explained simply by quenching of the hybridization gap as described above (it has the wrong sign), but may instead reflect anti-localization for this material, whose bulk resistivity $\rho_{xx} < h/e^2$ places it within the metallic regime. The in-plane field effect saturates above $B_\parallel = 1$ T, as expected for anti-localization when the Zeeman splitting exceeds relevant spin-orbit energies[21,22].

The weak in-plane field dependence of edge transport in InAs/GaSb samples has remained one of the most difficult aspects of the data to connect with the helical edge picture[6,8]. Both spin and orbital effects of the in-plane field should soften the hybridization gap, dramatically reducing the resistance in large (diffusive) devices. This significant in-plane field effect has never been observed. Similar results were obtained here by measuring the magnetoresistance of the trivial edge channels. In our experiments only the most resistive device [the Hall bar of Fig. 2] showed significant in-plane field dependence in the trivial regime: a factor-of-two reduction in resistance at high field in region I [Fig. 5(b)]. The in-plane field dependence was less than 10% for all other devices measured [see, for example, Fig. 7(e)]. This extreme sample-to-sample variability is not yet understood, but is consistent with an origin extrinsic to the edge states themselves. It may also reflect the wide variation of in-plane field dependences observed for variable range hopping that results from a competition between orbital and spin effects[23].

IV. MICROSCOPIC SAMPLES

A. Two Terminal Device

Given the similarity between observations of edge transport in our samples, compared to those reported to be in the QSH regime, we next investigate whether the edge channels responsible for the data in Fig. 2 are single-mode, as expected for the spin-resolved edge states of a QSH insulator. Helical edge channels are expected to have quantized conductance, e^2/h for each edge, for edges shorter than a characteristic spin flip length for the electrons[1,8,10,11]. This length has been reported to be several microns in previous work[8]. We tested the quantization of edge channel conductance in our samples using two devices with a geometry similar to that shown in Fig. 6(a): long InAs/GaSb mesas of width W ($W = 1$ μm and $W = 2$ μm for the two devices), across which multiple gates of length L are patterned. The length L of each gated region along the Hall bar ranged from 300 nm to 20 μm.

Starting with all gates grounded ($V_{BG} = 0$, and no top gate or $V_{TG} = 0$ at all locations) the entire mesa was in the n-doped regime and highly conductive. By monitoring the mesa resistance end-to-end while energizing one gate at a time, thereby bringing the region under the energized gate into the trivial insulating regime, we could then determine the edge resistance vs length in a single device. The effect of various top gates on

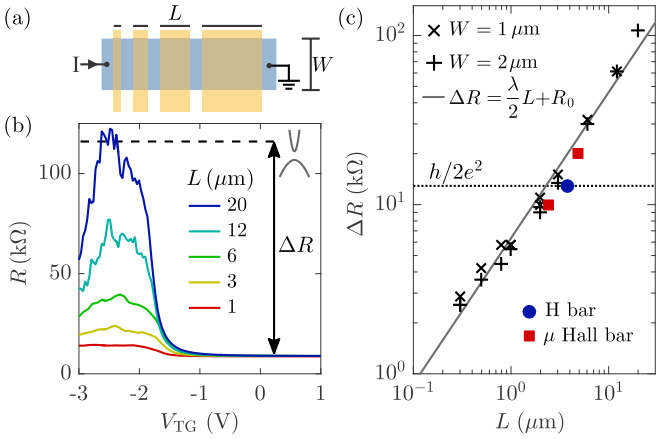

FIG. 6. (a) Schematic representation of the two-terminal device and the electric setup used to measure the length dependence of the edge channel resistance. (b) Resistance of the $W = 2$ μm sample as a function of top gate voltage $V_{\rm TG}$ for top gates of different lengths L. (c). Resistance change in the two-terminal device as a function of gate length for the $W = 1$ μm (crosses) and $W = 2$ μm (plus signs) together with a linear fit (black line). Circles and squares indicate the edge resistances measured in the H bar and μ Hall bar respectively, as discussed in Sec. IV B.

the two-terminal mesa resistance R is shown in Fig. 6(b) ($W = 2$ μm). The resistance change ΔR measured from the resistance peak ($V_{\rm TG} \sim -2.2V$) to the highly conductive n-type regime ($V_{\rm TG} > 0V$) represents the resistance of a two-terminal sample with length equivalent to the gate width L. The residual length-dependent bulk contribution due to the bulk resistance at positive $V_{\rm TG}$ is not considered in this analysis as negligible ($< 1\%$) compared to ΔR.

The quantity ΔR is seen to be directly proportional to L (Fig. 6c) throughout the range 300 nm$\leq L \leq 20$ μm, and independent of the mesa width W (crosses and plus signs for $W = 1$ μm and $W = 2$ μm respectively). The insensitivity of the two-terminal resistance to sample width provides further evidence that current exclusively flows along the edges. The resistance change ΔR is fit with the functional form $\Delta R = 1/2\ \lambda L + R_0$ where λ is the resistance per unit length of one edge channel, the factor 1/2 takes into account two edge channels that conduct in parallel, and R_0 is the resistance minimum in the short-channel limit. The fit (solid line) results in $\lambda = 10.4$ k$\Omega\mu$m^{-1} and $R_0 \approx 0$. We will comment further on these results in Sec. VI.

B. H Bar and Microscopic Hall Bar

One of the strongest arguments in favor of a QSH interpretation for edge channel conduction in previous InAs/GaSb measurements has been the fact that the local and non-local resistances of micron-scale structures are close to the quantized values predicted for single-mode edges. The majority of such measurements have been in so-called H bar geometries, or in microscopic Hall bars with micron-scale separations between leads[6,8,10,11]. Notwithstanding the arguments for a non-topological interpretation for edge channel conduction in our samples, the characteristic local and non-local resistances for micron-scale devices in our samples [Figs. 7(a) and 7(b)] were nevertheless close to those predicted from a Landauer-Buttiker analysis of single-mode edges.

The H bar device, schematically shown in Fig. 7(a), has a length of 3.8 μm (defined by the top gate) and the width of its arms is 1 μm. This geometry is nearly identical to those reported in Refs. 8 and 11. The resulting H shape connects adjacent pairs of n-doped contacts by edges each having a length of 3.8 μm. Figure 7(c) shows various four terminal resistance $R_{ij-lm} = V_{ij}/I_{lm}$, measured by passing a current I_{lm} between terminal l and m and by measuring the voltage drop V_{ij} between contact i and j. When the top gate drives the bulk into the insulating regime ($V_{\rm TG} < -3$ V), the resistance saturates to a plateau that depends on the particular set of contacts used for the measurement.

The plateau resistances are very close to the quantized values expected in this geometry for perfectly transmitting helical (single-mode) edge channels, as calculated using Landauer-Büttiker formalism[11,24]. The configuration V_{14}/I_{14} (blue line) can be modeled as one h/e^2 resistor (direct path from 1 to 4) in parallel with three h/e^2 resistors in series, yielding a total resistance of $3h/4e^2$. Similar arguments hold for the other three curves shown in Fig. 7(c). The four terminal resistance V_{23}/I_{14} (orange line) measures exclusively the non-local response of the edge channel. When the sample is in the n-type regime (i.e. for $V_{\rm TG} > -3$ V), V_{23}/I_{14} vanishes. For $V_{\rm TG} < -3$ V, a plateau at $h/4e^2$ forms offering further evidence that, also in the H bar, transport in the insulating regime is exclusively mediated by edge channels. The symmetric configuration V_{13}/I_{24} (red line) results in a zero resistance plateau. The zero resistance plateau indicates that the currents moving on opposite sides of the H bar are balanced. We stress that this analysis assumes single mode channels, which the length dependent measurements presented in the previous section appear to rule out. We are therefore left to interpret this apparent resistance quantization [Fig. 7(c)] as coincidental, due to a particular edge channel resistance of 25.8 k$\Omega \approx h/e^2$.

The same type of analysis is performed on a sample with a more conventional Hall bar geometry where the separation between adjacent contacts is on the micron-scale, shorter than previously reported relaxation lengths. The μ Hall bar, shown in Fig. 7(b), has eight lateral arms, a width of 1 μm and a length of 12 μm (defined by the top gate). The separation between contact 2 and 3 and between 3 and 4 is 2.4 μm while the separation between contact 4 and 5 is 4.8 μm. The sample is measured by passing a current I_{16} between contact 1 and 6 and measuring the voltage drop between couples of lateral arms. In case of perfectly transmitting helical edge

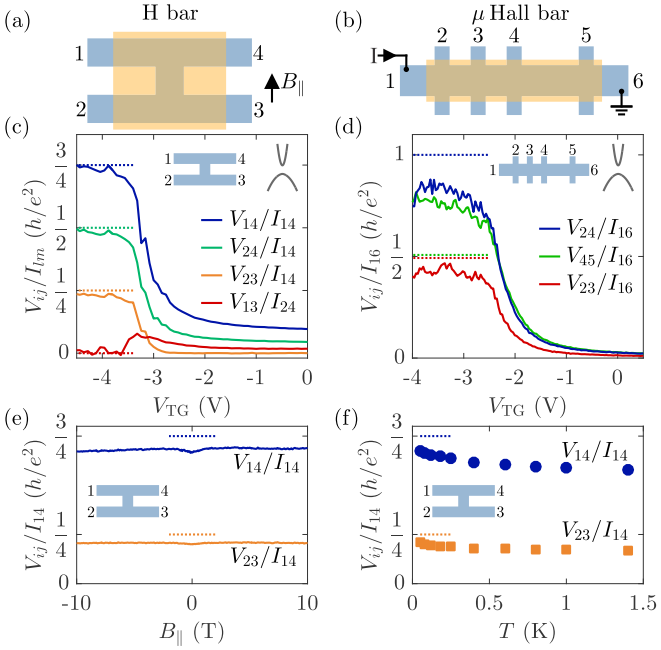

FIG. 7. (a) Schematic representation of the H bar geometry with the contact numbering used in (c), (e) and (f). (b) Schematic representation of the μ Hall bar, the electrical setup and the contact numbering used in (d). (c) Four terminal resistances measured in the H bar geometry as a function of top gate voltage in different contact configurations. (d) Four terminal resistances measured in the μ Hall bar geometry as a function of top gate voltage for different contact configurations. (e) Two H bar four terminal resistances at $V_{TG} = -4$ V as a function of in-plane magnetic field. The field orientation is shown in (a). (f) Same as in (e) as function of temperature. Dotted lines in (c), (d), (e) and (f) indicate the expected resistances in case of helical edge channels.

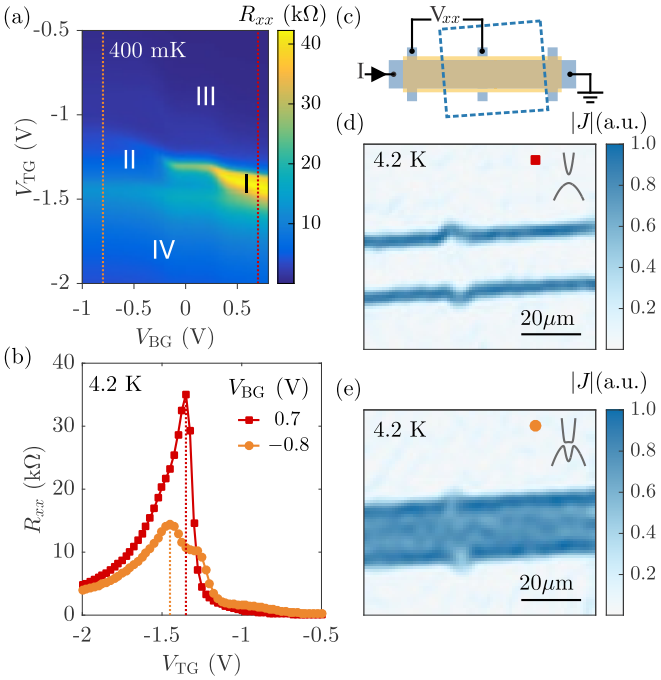

FIG. 8. (a) Four-terminal longitudinal resistance R_{xx} as a function of top gate (V_{TG}) and back gate voltage (V_{BG}). For clarity, a higher resolution 2D plot taken at 400 mK is shown in lieu of one taken at 4.2 K, the same temperature as the images. (b) Resistance traces vs. V_{TG} taken at 4.2 K for different back gate voltages V_{BG}, as indicated by the dotted lines in (a). (c) Schematic representation of the measurement setup. The dashed box indicates the imaged area. (d,e) Scanning SQUID images of the absolute value of the current density $|J|$, acquired in the high resistance non-inverted regime (d) and lower resistance, inverted regime (e). The images were taken at back gate voltages indicated in (b) by the dashed lines.

channels, the four terminal resistance would be $h/2e^2$ if measured between adjacent lateral arms (independently of their spatial separation). If measured between two lateral arms separated by a third one acting simply as a dephasing probe, the four terminal resistance would rise to h/e^2. Contrary to these expectations, as shown in Fig. 7(d), the measured resistance depends exclusively on length, and is not dependent on the number of intervening voltage probe contacts. In particular, V_{23}/I_{16} (red line, 2.4 μm) is half of V_{45}/I_{16} (green line, 4.8 μm), while they should both be quantized at $h/2e^2$. Similarly, the presence of an unused voltage probe between contacts 2 and 4 does not elevate the resistance V_{24}/I_{16} (blue line,4.8 μm) above V_{45}/I_{16} (green line, 4.8 μm), for which there is no voltage probe between contacts.

The local and non-local resistances of the H bar were found to depend much less strongly on temperature or in-plane field as compared to analogous measurements in the macroscopic Hall bar. Figure 7(e) and (f) show the V_{14}/I_{14} and V_{23}/I_{14} configurations for a constant top gate voltage $V_{TG} = -4$ V as a function of $B_\parallel$ and T respectively. The resistance of the edge channels does not show any significant field dependence up to 10 T, except a weak positive magnetoresistance close to $B_\parallel = 0$. We interpret these observations as consistent with the evolution from a temperature independent regime above 0.5 K to a weakly insulating dependence approaching low temperatures.

V. SCANNING SQUID MEASUREMENTS

The conducting edge channels identified above were also spatially imaged using scanning SQUID microscopy. The SQUID used to image current had a 3 μm diameter pickup loop[25]. An alternating current was applied to the sample [Fig. 8(c)] and the AC flux response was measured through the SQUID's pickup loop as a function of position. Using Fourier techniques and our SQUID experimentally-extracted point spread function[11,26], the 2D current density was obtyained directly from AC flux images. The images in Fig. 8 present the absolute value of the 2D current density, which in this geometry is

roughly proportional to the local conductivity. Current density images were taken at 500 $\mathrm{nA_{rms}}$, which is rather high compared to currents used in standard transport measurements. The shape of flux line cuts in the trivial regime did not change as a function of applied current, down to 50 $\mathrm{nA_{rms}}$. The relatively high bias (up to 10 mV across the voltage probes) of these measurements most likely masks any non-linear effects present at lower biases[18]. For this experiment, unintentional RC filtering from the wiring had not been well characterized at the frequencies of the applied current, so the extracted current density images are plotted in arbitrary units (A.U.). Transport measurements on the device imaged by SQUID were taken at 10 $\mathrm{nA_{rms}}$ and low frequencies ($\approx$ 10 Hz), using the contacts indicated in Fig. 8(c).

The gate voltage map of resistance for wafer C [Fig. 8(a)] was qualitatively but not quantitatively similar to the analogous maps for wafer A previously presented in Figs. 1, 2, and 3. Thorough magnetotransport studies of wafer C from Ref. 9, covering similar gate voltage ranges, confirms the labeling of the phase diagram into regions I, II, III, IV as in Fig. 1. Resistance peaks as a function of top gate voltage [Fig. 8(b)] identify the alignment of the Fermi energy within the inverted and trivial gaps. In the trivial regime, the resistance rises only to 35 kΩ [Fig. 8(b)] compared to hundreds of kΩ observed in wafer A. In the inverted regime, the resistance peak is around $R_{xx} \sim 15$ kΩ compared to 40 kΩ in wafer A. Note that the 2D resistance plot in Fig. 8(a) is taken at 400 mK, whereas the scanning images [Fig. 8(d,e)] are measured at 4.2 K. The transport data at 4.2 K is qualitatively similar [see Fig. 9(b)], although the resistance peak in the trivial regime is lower.

The main scanning SQUID results are presented in Figs. 8(d,e). In Fig. 8 images were taken far from the point of band gap closing, near the largest positive and negative values of V_{BG} applied. Specifically, current was imaged at the maximum resistance at fixed back gate voltages $V_{\mathrm{BG}} = 0.7$ V (trivial) and $V_{\mathrm{BG}} = -0.8$ V (inverted), indicated by the dashed red and yellow lines in Fig. 8(a). In the trivial regime, current flowed exclusively on the edge of the sample [Fig. 8(c)], consistent with the conclusion reached from the transport data presented above. Even at the small overlap between the top-gate and the voltage leads [see Fig. 8(c)] current flows along the edge of voltage probes until it reaches the ungated n-type region. When the Fermi energy was far from the gap, in either the n-type or p-type conducting regimes III or IV of the phase diagram, no edge currents were observed (not shown).

In the inverted regime ($V_{\mathrm{BG}} = -0.8$ V), enhanced current density along the edges of the device was also observed, but concomitantly to measurable current flow in the bulk. This is consistent with what was observed previously in undoped InAs/GaSb with scanning SQUID[7], and explained by the residual bulk conductivity in hybridization gap, as confirmed by Corbino measurements [Figs. 3 and 4]. The measurements in the inverted regime

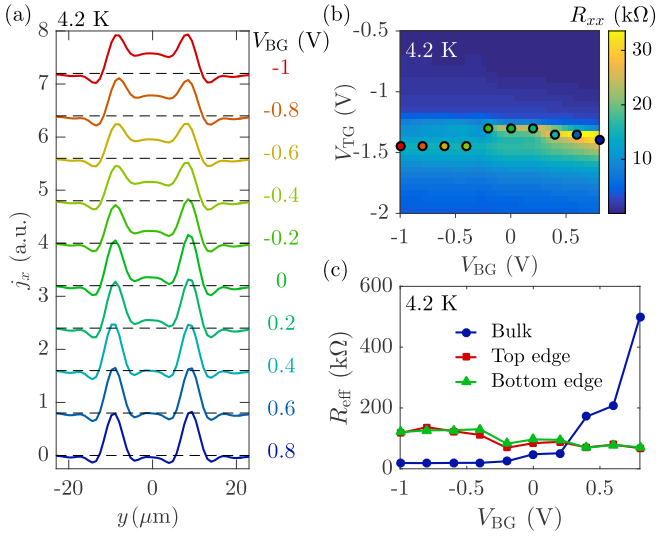

FIG. 9. (a) Line cuts of current density j_x extracted from averaged flux line cuts as a function of back gate voltage. The line cuts are offset for clarity. Each line cut was taken at the resistance maximum of the top gate sweep, which is not necessarily the charge neutrality point in the inverted regime. The applied current was $I = 100$ $\mathrm{nA_{rms}}$. (b) Longitudinal resistance taken at $T = 4.2$ K. The gate voltages at which the line cuts of (a) were taken are indicated by the corresponding markers. (c) Effective resistance R_{eff} extracted from fitting flux line cuts and the measured R_{xx}.

were performed at the maximum resistance, which in this case might coincide with the onset of electron-hole hybridization, as in Fig. 5(a), rather than the middle of the gap. The presence of edge channels throughout the gap has been established by scanning SQUID previously in InAs/GaSb[7], and therefore the presence of edge channels here, even if the Fermi level is not well-centered in the hybridization gap, is not surprising.

Conducting edges were observed across the phase diagram in the gapped regions at all of the back gate voltages which were investigated [see Fig. 9]. For the chosen values of V_{BG}, V_{TG} was set in order to maximize the value of R_{xx} and then the magnetic flux from the Hall bar was imaged along a line perpendicular to the current flow ('flux line cuts'). The positions in gate space where the flux line cuts were taken are indicated on the resistance color plot of Fig. 9(b). The flux line cuts were converted into current density along the Hall bar axis, j_x, using methods described elsewhere[7]. The result of this analysis is shown in Fig. 9(a). Edge states were present throughout the entire phase diagram (on the resistance peaks), and the current along the edges and in the center of the device varied smoothly as a function of V_{BG}. The bulk current was nearly zero in the non-inverted regime ($V_{\mathrm{BG}} = 0.8$ V), and rose smoothly above zero as the gate voltage was tuned into the inverted regime.

In order to quantify the dependence of the current distribution on V_{BG}, the flux line cuts of Fig. 9(a) were fitted to determine the fraction of current F flowing in

the top edge, bottom edge and bulk of the Hall bar ($F_{\rm top}$, $F_{\rm bot}$, $F_{\rm bulk}$). Assuming each of the three channels contributes to transport in parallel, their effective resistances are given by $R_{\rm eff} = R_{xx}/F_{\rm top,bot,bulk}$ (for more details see Ref. 7). The results of this analysis are shown in Fig. 9(c). Consistent with previous observations, the effective resistance of the bulk strongly increased at positive $V_{\rm BG}$, indicating an opening of the trivial gap. On the other hand, in the inverted regime we found that the bulk effective resistance does not change significantly as a function of $V_{\rm BG}$. Additionally, there is not a strong decrease in the bulk resistance in between the two regimes, as one would expect for a gap closing. Both of these features are at least partially explainable by the residual bulk conductivity in the inverted regime. Despite the transition from inverted to non-inverted regime, the edges effective resistance varied only up to a factor of two between the highest and lowest $V_{\rm BG}$ values. In particular, the edges resistance smoothly changed across the region where the gap should close, consistent with the edges observed in the non-inverted regime persisting into the inverted regime. It is possible, however, that the similarity in the resistance of the edges in the two regimes is accidental, and that the trivial edge states disappear only close to the gap closing. More detailed work near the gap closing is warranted, especially at lower biases and temperature, but these measurements indicate that the presence of trivial edge states in the inverted regime, in addition to the trivial regime, is certainly possible.

VI. DISCUSSION

The ability to tune between inverted and trivial regimes using top and back gate voltages enables a determination of the sample band structure topology for a given set of conditions[9]. As outlined above, however, we observe several surprising characteristics of the trivial phase for this sample.

First, the temperature dependence of the bulk conductivity measured in Corbino geometry implies an energy gap $\Delta \leq 8$K that is surprisingly small compared to theoretical expectations[2,20]. Using a parallel plate capacitor model[9], the estimated energy gap at $V_{\rm BG} = 0$ would be 300 K assuming that electron and hole wavefunctions sit in the center of the respective QWs, and that the gap closes when $V_{\rm BG} = -1$ V [this backgate voltage corresponds to the tip of the trivial phase in Fig. 3(a)]. The two orders of magnitude discrepancy between the measured and estimated energy gap in the trivial regime is yet not understood. The electron and hole wavefunctions separation could be much smaller than the QWs thickness or, as observed in bilayer graphene, disorder may result in a large underestimate of the energy gap size measured in a transport experiment[27,28].

Most significantly, edge channels are consistently observed in the trivial regime, both in transport and in scanning SQUID images. The non-topological character of these edges is supported by measurements, indicating that the edge channel resistance scales linearly with length down to a length of at least 300 nm, at which point the resistance is far below the $h/2e^2 \approx 12.9$ kΩ, expected for single-mode conducting channels [Fig. 6(c)]. The resistance of a QSH sample can increase above $h/2e^2$ in case of spin scattering between counterpropagating edges, but it can not assume lower values (assuming no bulk conduction). Ballistic, single-mode non-helical edge channels would yield a minimum resistance $h/4e^2 \approx 6.4$ kΩ for lengths less than or comparable to the elastic mean free path. With a minimum measured $\Delta R \approx 3$ kΩ that falls well below this lower bound, we conclude that our edge channels are composed of at least 2 spin-degenerate modes, with a mean free path shorter than 300 nm.

It is worth noting that our observation of edge channels in the trivial regime does not exclude the possibility of finding helical edges in the inverted regime, but in the present samples bulk conduction is too high for these to be observed in a transport experiment. On the other hand, scanning SQUID images offer evidence of enhanced edge conduction in the inverted regime that continuously evolves to edge states in the trivial regime. Indeed, one of the primary points to be taken from this work is that trivial edge modes are likely to be found in InAs/GaSb QW systems, conducting in parallel with any helical edge modes that might appear in inverted band-structure regime. These modes are consistently observed in the conventional insulating state, and should likely be present in the inverted regime too where (hybridization) band gaps are much smaller.

The non-helical edge conduction we report is robust in the sense that it was observed for many different samples made on three different wafers and processed in three different laboratories, using different top gate insulators and slightly different processing recipes. This indicates that edge conduction may be a common feature of InAs/GaSb quantum wells. At the same time, quantitative details of the edge conductance did appear to depend on precise processing conditions. For example, the linear edge resistivity λ was identical for the two two-terminal devices of Sec. IV A: $\lambda = 10.4$ kΩμm^{-1} at $T = 50$ mK. These devices were patterned on the same chip and processed at the same time. The macroscopic Hall bar described in Fig. 2 was fabricated on a different chip from the same wafer, and processed in a different fabrication run; the linear edge resistivity of this device was $\lambda = 26.4$ kΩμm^{-1}. The H bar and the μ-Hall bar, patterned together on a third chip from the same wafer, gave $\lambda = 8$ kΩμm^{-1} (circles and squares in Fig. 6 for the H and μ-Hall bar respectively).

The temperature dependence and in-plane field dependence of λ was also different for samples processed in different batches. Edge channels showed an insulating temperature dependence ($\partial\lambda/\partial T < 0$) in every sample, but the magnitude of the variation with temperature was much stronger in the macroscopic Hall bar [see Fig. 4(c)]. The in-plane field dependence of the macroscopic Hall

bar was also much stronger: a factor of two resistance decrease in a 5 T field [see 5(b)], compared to a $< 5\%$ change for the H bar and the two terminal devices. The general magnetic field dependence is not consistent with QSH edge channels, where the breaking of time reversal symmetry is expected to induce back scattering.

The processing-dependent linear resistance of the edge channels in these devices may give a hint to their origin. For example, band bending of the InAs conduction band at the vacuum interface can depend on the precise termination of the semiconductor crystal. This effect is typically of the order of the bulk InAs energy gap[29–31]. Because of the very small energy gap in the double QW system close to the inverted-trivial transition, band bending might therefore be particularly relevant and lead to a significant charge accumulation at the etched edge of the samples. While our observations do not preclude the existence of a topological phase in the inverted regime of our samples (region II), observing exclusive helical edge channel transport would require controlling the bend bending of both electrons and holes to values smaller than the bulk hybridization gap.

Alternatively to band structure effects, spurious effects of the fabrication process might constitute the most relevant contribution to the creating of edge channels. As an example, the side walls of the mesa might become conducting due to a redeposition of amorphous Sb during AlSb etching, or to dangling bonds resulting from the exposure of the etched semiconductor to air[32,33]. Such problems have been widely studied in the field of optoelectronics, and various passivation techniques were proposed[34].

We note that band bending at the sample edges is a phenomenon that has been observed for other small band gap materials. Graphene, for example, exhibits enhanced edge conduction close to the charge neutrality point, as was observed via superconductive interferometry measurements[35]. It was also recently demonstrated that inverted HgTe/CdTe QWs also show edge channels whose conductance properties are inconsistent with the common expectations of a QSH insulator[36]. The authors of Ref. 36 also speculated that, in the case of HgTe/CdTe, extrinsic effects may cause an enhanced conductance close to the sample edges.

Enhanced conductance can also arise due to electric field focusing at the sample edges[37]. This effect may be particularly relevant for top gates deposited after etching, resulting in conformal coverage of the etched walls. Because of the higher top gate capacitance at the mesa walls, the edges can be brought to a conductive p-type regime for a top gate voltage at which the bulk is still insulating.

If the sample edges have finite carrier density due to band bending or other effects in the trivial regime, one might consider depleting them using side gates. Preliminary results have indicated that side-gating the edges partially reduces edge conduction but not completely, and the sign of the effect indicates that the carriers are n-type.

Recent measurements of Si-doped InAs/GaSb QWs in other groups have confirmed the coexistence of an insulating bulk with conductive edge channels[6–8]. Similar to the measurements reported here, the resistance of the edge channels scaled linearly with length, with $\lambda \approx 6$ k$\Omega\mu$m^{-1}. The samples presented in Ref. 6–8 were claimed to be in the inverted regime, whereas the measurements reported here are for samples whose regime (inverted or trivial) can be changed using gate voltages. The most significant contrast between earlier reports[8] and the measurements reported here is the observation of conductance quantization to within 1% of the expected value for three devices with edge lengths somewhat shorter than the typical scattering length scale $\lambda_\varphi \approx 4.4$ μm[8]. The more extensive measurement of length dependence reported here, extending down to lengths an order of magnitude shorter than λ_φ, enabled a clear determination that in our samples the apparent quantization of edge resistance was accidental.

VII. CONCLUSION

We have shown that edge channel transport in InAs/GaSb, previously described in the literature as a signature of helical states, can also be seen in the trivial (non-topological) regime. Quantitative metrics of the edge transport in our samples, with non-inverted band structure, are nearly identical to those described in earlier reports. Two experimental observations, however, allow us to conclude unambiguously that the edge conduction reported here is of a different nature than that predicted in the framework of the QSH effect: First, we explore the entire phase diagram of our samples via gate voltages, and thereby identify the parameter space where edge conduction is observed to be one where the band structure is trivial, that is, not inverted. Second, short edge channels segments have a resistance much smaller than h/e^2, indicating they are composed of many modes with a short scattering length.

Our results highlight the importance of considering enhanced edge conduction in broken gap materials, where the energy gap might be comparable to band bending at an interface. Trivial edges result in a behavior remarkably similar to those expected from a QSH insulator, hence proper characterization of the edge channels nature is crucial. Our measurements and analysis provide one example of an experimental framework for distinguishing between trivial and helical edge states.

ACKNOWLEDGMENTS

This work was supported from Microsoft Corporation Station Q. The work at Copenhagen was also supported by the Danish National Research Foundation and Villum Foundation. The work at Delft was also supported

by funding from the Netherlands Foundation for Fundamental Research on Matter (FOM). The work at Stanford was supported by the Department of Energy, Office of Basic Energy Sciences, Division of Materials Sciences and Engineering, under Contract No. DE-AC02-76SF00515. F.N. acknowledges support of the European Community through the Marie Curie Fellowship, grant agreement No 659653. J.F. and E.S. acknowledge support from QMI, NSERC, and CFI.

* email: fnichele@nbi.ku.dk

[1] B. A. Bernevig, T. L. Hughes, and S.-C. Zhang, Science **314**, 1757 (2006).
[2] C. Liu, T. L. Hughes, X.-L. Qi, K. Wang, and S.-C. Zhang, Phys. Rev. Lett. **100**, 236601 (2008).
[3] I. Knez, R.-R. Du, and G. Sullivan, Phys. Rev. Lett. **107**, 136603 (2011).
[4] K. Suzuki, Y. Harada, K. Onomitsu, and K. Muraki, Phys. Rev. B **87**, 235311 (2013).
[5] F. Nichele, A. N. Pal, P. Pietsch, T. Ihn, K. Ensslin, C. Charpentier, and W. Wegscheider, Phys. Rev. Lett. **112**, 036802 (2014).
[6] I. Knez, C. T. Rettner, S.-H. Yang, S. S. P. Parkin, L. Du, R.-R. Du, and G. Sullivan, Phys. Rev. Lett. **112**, 026602 (2014).
[7] E. M. Spanton, K. C. Nowack, L. Du, G. Sullivan, R.-R. Du, and K. A. Moler, Phys. Rev. Lett. **113**, 026804 (2014).
[8] L. Du, I. Knez, G. Sullivan, and R.-R. Du, Phys. Rev. Lett. **114**, 096802 (2015).
[9] F. Qu, A. J. Beukman, S. Nadj-Perge, M. Wimmer, B.-M. Nguyen, W. Yi, J. Thorp, M. Sokolich, A. A. Kiselev, M. J. Manfra, C. M. Marcus, and L. P. Kouwenhoven, Phys. Rev. Lett. **115**, 036803 (2015).
[10] M. König, S. Wiedmann, C. Brüne, A. Roth, H. Buhmann, L. W. Molenkamp, X.-L. Qi, and S.-C. Zhang, Science **318**, 766 (2007).
[11] A. Roth, C. Brne, H. Buhmann, L. W. Molenkamp, J. Maciejko, X.-L. Qi, and S.-C. Zhang, Science **325**, 294 (2009).
[12] C. Charpentier, S. Falt, C. Reichl, F. Nichele, A. N. Pal, P. Pietsch, T. Ihn, K. Ensslin, and W. Wegscheider, Appl. Phys. Lett. **103**, 112102 (2013).
[13] S. Mueller, A. N. Pal, M. Karalic, T. Tschirky, C. Charpentier, W. Wegscheider, K. Ensslin, and T. Ihn, Phys. Rev. B **92**, 081303 (2015).
[14] B.-M. Nguyen, W. Yi, R. Noah, J. Thorp, and M. Sokolich, Applied Physics Letters **106**, 032107 (2015).
[15] M. J. Yang, K. A. Cheng, C. H. Yang, and J. C. Culbertson, Applied Physics Letters **80**, 1201 (2002).
[16] F. Nichele, *Transport experiments in two-dimensional systems with strong spin-orbit interaction*, Ph.D. thesis, ETH-Zürich (2014).
[17] D. A. Abanin, S. V. Morozov, L. A. Ponomarenko, R. V. Gorbachev, A. S. Mayorov, M. I. Katsnelson, K. Watanabe, T. Taniguchi, K. S. Novoselov, L. S. Levitov, and A. K. Geim, Science **332**, 328 (2011).
[18] T. Li, P. Wang, H. Fu, L. Du, K. A. Schreiber, X. Mu, X. Liu, G. Sullivan, G. A. Csáthy, X. Lin, and R.-R. Du, ArXiv e-prints (2015), arXiv:1507.08362 [cond-mat.mes-hall].
[19] A. L. Efros and B. I. Shklovskii, Journal of Physics C: Solid State Physics **8**, L49 (1975).
[20] M. J. Yang, C. H. Yang, B. R. Bennett, and B. V. Shanabrook, Phys. Rev. Lett. **78**, 4613 (1997).
[21] I. L. Aleiner and V. I. Fal'ko, Phys. Rev. Lett. **87**, 256801 (2001).
[22] F. E. Meijer, A. F. Morpurgo, T. M. Klapwijk, and J. Nitta, Phys. Rev. Lett. **94**, 186805 (2005).
[23] L. Ioffe and B. Spivak, *Journal of Experimental and Theoretical Physics*, Journal of Experimental and Theoretical Physics **117**, 551 (2013).
[24] M. Büttiker, Phys. Rev. B **38**, 9375 (1988).
[25] M. E. Huber, N. C. Koshnick, H. Bluhm, L. J. Archuleta, T. Azua, P. G. Björnsson, B. W. Gardner, S. T. Halloran, E. A. Lucero, and K. A. Moler, Review of Scientific Instruments **79**, 053704 (2008).
[26] K. C. Nowack, E. M. Spanton, M. Baenninger, M. König, J. R. Kirtley, B. Kalisky, C. Ames, P. Leubner, C. Brüne, H. Buhmann, L. W. Molenkamp, D. Goldhaber-Gordon, and K. A. Moler, Nat. Mater. **12**, 787 (2013).
[27] T. Taychatanapat and P. Jarillo-Herrero, Phys. Rev. Lett. **105**, 166601 (2010).
[28] H. Min, D. S. L. Abergel, E. H. Hwang, and S. Das Sarma, Phys. Rev. B **84**, 041406 (2011).
[29] D. C. Tsui, Phys. Rev. Lett. **24**, 303 (1970).
[30] M. Noguchi, K. Hirakawa, and T. Ikoma, Phys. Rev. Lett. **66**, 2243 (1991).
[31] L. O. Olsson, C. B. M. Andersson, M. C. Håkansson, J. Kanski, L. Ilver, and U. O. Karlsson, Phys. Rev. Lett. **76**, 3626 (1996).
[32] C. Gatzke, S. J. Webb, K. Fobelets, and R. A. Stradling, Semiconductor Science and Technology **13**, 399 (1998).
[33] R. Chaghi, C. Cervera, H. At-Kaci, P. Grech, J. B. Rodriguez, and P. Christol, Semiconductor Science and Technology **24**, 065010 (2009).
[34] E. A. Plis, M. N. Kutty, and S. Krishna, Laser & Photonics Reviews **7**, 45 (2013).
[35] M. T. Allen, O. Shtanko, I. Cosma Fulga, A. Akhmerov, K. Watanabi, T. Taniguchi, P. Jarillo-Herrero, L. S. Levitov, and A. Yacoby, ArXiv e-prints (2015), arXiv:1504.07630 [cond-mat.mes-hall].
[36] E. Y. Ma, M. R. Calvo, J. Wang, B. Lian, M. Muhlbauer, C. Brune, Y.-T. Cui, K. Lai, W. Kundhikanjana, Y. Yang, M. Baenninger, M. Konig, C. Ames, H. Buhmann, P. Leubner, L. W. Molenkamp, S.-C. Zhang, D. Goldhaber-Gordon, M. A. Kelly, and Z.-X. Shen, Nat Commun **6**, (2015).
[37] I. J. Vera-Marun, P. J. Zomer, A. Veligura, M. H. D. Guimares, L. Visser, N. Tombros, H. J. van Elferen, U. Zeitler, and B. J. van Wees, Applied Physics Letters **102**, 013106 (2013).